AL BIGHTS RESERVE: REPOOLUTION OR DISCUSSING TO THIS PARTIES OF ANY ART OF THIS     BETTER IS IN TRANSPORT IN THE WITTEN PROMISION OF PORCE. WWW RV.     BETTER IS OF PORCE. I PRODUCTION OF DISCUSSING OF PORCE. WWW RV.     BETTER IS OF PORCE. I PRODUCTION OF DISCUSSING OF PORCE. WWW RV.     BETTER IS OF PORCE. I PRODUCTION OF DISCUSSING OF PORCE. WWW RV.     BETTER IS OF PORCE. WWW RV.     BETTER IS OF PORCE. I PRODUCTION OF DISCUSSING OF PORCE. WWW RV.     BETTER IS OF PORCE. WWW RV.     BETTER IS OF PORCE.     BETTER IS OF	
ALL BIGHTS RESERVED: REPRODUCTION OR DISCLOSURE TO THIRD PARTIES OF ANY PART OF THIS         REPORT IS NOT FERMITTED, EXCEPT WITH THE WRITTEN PERMISSION OF FORCEL-WAY B.Y.         PREVENT CB-AP       UTGAVE         INSUE       1         INSUE       DATE         DATE       DATE         INDERVISION       CB-AP         INDERVISION       DATE         DATE       DATE         DATE       1979 - 2013         BALL BIOLENCIA       DATE         DATE       1979 - 2013         BALEGOT       Static Directional Stability and Control of Transport Aircraft         INDERVISION       An analysis is described of side-force and yawing-moment-in-sideslip of conventional transport aircraft based on available wind tunnel and full-size aircraft data.         After a chapter on general design requirements the analysis is divided in a part which describes the contribution of the tail surfaces to side-force and yawing-moment-due-to- sideslip. Particular attention is paid to the different contributions to the sidewash as experienced by the tail surfaces. Also rudder characteristics are discussed.         PREVENTED       E.Obert       DETEN AKOORD         DATE       INTERNAL APROVED       EXEMPTION         BERNAMING / MOTO MOS.       THE INFORMATION         TERMING / FOTO MIS.       THE INFORMATION	2.4
BEORT IS NOT PERMITTED, BLOEP WITH HE WINTER PERMITTED CONTOURS     CB-AP     UTCAVE     I     BAPTORT NO. A-128     BAPTORT NO. AND A ANALYSIS IS DEVOLVED     BERORTROLEED     BAPTORT NO. AND A ANALYSIS IS DEVOLVED     BAPTORT NO. A-128     BAPTORT NO. AND A ANALYSIS IS A BAPTORY NO. A ANALYSIS IS BAPTORY NO. A ANALYSIS IS A BAPTORY NO. A ANALYSIS IS A BAPTORY NO. A ANALYSIS IS A BAPTORY AND A ANALYSIS IS A BAPTORY AND A ANALYSIS A BAPTORY AND A ANALYSIS A BAPTORY AND A ANALYSIS A BAPTORY AND A BAPTORY AND A ANALYSIS A BAPTORY AND A BAP	
PRELING EPARTMENT       CB-AP       UTCAVE ISSUE       1       RAPPORT NO. BEORY NO.       A-128         UBRICENTING EVENTY       DATUM DATE       1979 - 2013       NO.       A-128         NOEWVERP UBECT       Static Directional Stability and Control of Transport Aircraft         An analysis is described of side-force and yawing-moment-in-sideslip of conventional transport aircraft based on available wind tunnel and full-size aircraft data. After a chapter on general design requirements the analysis is divided in a part which describes the tail-off characteristics and a part which describes the contribution of the tail surfaces to side-force and yawing-moment-due-to- sideslip. Particular attention is paid to the different contributions to the sidewash as experienced by the tail surfaces. Also rudder characteristics are discussed.         PREFARED ECODET       ECODET       CREMINGLEED CHERNAL APPROVED       ENTERNAL APPROVED         INTERNAL APPROVED       ENTERNAL APPROVED       ENTERNAL APPROVED       ENTERNAL APPROVED         TERNING / FOID NRS. CONTROLLED DOPY       TER INFORMATION       ENTERNAL APPROVED       ENTERNAL APPROVED	
DRATE         DATIM         1979 – 2013         BLAD PAGE         1           INDERIVERPATION INDEET         Static Directional Stability and Control of Transport Aircraft         1           INDERIVERPATION INDEET         Static Directional Stability and Control of Transport Aircraft         1           An analysis is described of side-force and yawing-moment-in-sideslip of conventional transport aircraft based on available wind tunnel and full-size aircraft data. After a chapter on general design requirements the analysis is divided in a part which describes the tail-off characteristics and a part which describes the contribution of the tail surfaces to side-force and yawing-moment-due-to- sideslip. Particular attention is paid to the different contributions to the sidewash as experienced by the tail surfaces. Also rudder characteristics are discussed.           OPOSITED INTERNAL APPROVED         EXEMPTION           BATEN         INTERNAL APPROVED           BERMANTE INTERNAL APPROVED         EXEMPTION           BERMANTE INTERNAL APPROVED         EXTERNAL APPROVED           BERMANTE INTERNAL APPROVED         EXTERNAL APPROVED           BERMAND / FOTO MRS. COMMING / PHOTO MOTS.         TER INFORMATIE FOR INFORMATION	
Static Directional Stability and Control of Transport Aircraft         NDERWERP UNEART         Static Directional Stability and Control of Transport Aircraft         AMENATTING         MARENATTING         Marena chapter on general design requirements the analysis is divided in a part which describes the tail-off characteristics and a part which describes the contribution of the tail surfaces to side-force and yawing-moment-due-to- sideslip. Particular attention is paid to the different contributions to the sidewash as experienced by the tail surfaces. Also rudder characteristics are discussed.         OPOSITED RECOMPTION DESCRETED         DECODERT         DECODERT         DECODERT         DETEN ADVOID	
AMERIATTING HUMMARY An analysis is described of side-force and yawing-moment-in-sideslip of conventional transport aircraft based on available wind tunnel and full-size aircraft data. After a chapter on general design requirements the analysis is divided in a part which describes the tail-off characteristics and a part which describes the contribution of the tail surfaces to side-force and yawing-moment-due-to- sideslip. Particular attention is paid to the different contributions to the sidewash as experienced by the tail surfaces. Also rudder characteristics are discussed. OPOESTIED E.Obert UTGAVE DATE	
An analysis is described of side-force and yawing-moment-in-sideslip of conventional transport aircraft based on available wind tunnel and full-size aircraft data. After a chapter on general design requirements the analysis is divided in a part which describes the tail-off characteristics and a part which describes the contribution of the tail surfaces to side-force and yawing-moment-due-to-sideslip. Particular attention is paid to the different contributions to the sidewash as experienced by the tail surfaces. Also rudder characteristics are discussed.   PREMARE  E.Obert  E.Obert E.	
transport aircraft based on available wind turner and united and un	
transport aircraft based on available Wind fullifier and full suffaces that each state analysis is divided in a part which describes the tail-off characteristics and a part which describes the contribution of the tail surfaces to side-force and yawing-moment-due-to- sideslip. Particular attention is paid to the different contributions to the sidewash as experienced by the tail surfaces. Also rudder characteristics are discussed.         POESTELD_EARD       E.Obert         DATUM       INTERNAL APPROVED         DATE       INTERNAL APPROVED         EXCENTIOLEERD_CONTROLEERD       CONTROLEERD         CONTROLEERD_CRECKED       CONTROLEERD         EXTERN AKKOORD       EXTERN AKKOORD         INTERNAL APPROVED       EXTERN AKKOORD         EXTERNAL APPROVED       EXTERNAL APPROVED         EXTERNAL APPROVED       CONTROLESE COPY         TERENING / POID NDS.       TER INFORMATIE         FOR INFORMATION       FOR INFORMATION	
After a chapter on general design requirements the analysis of exercises the contribution of the describes the contribution of the tail surfaces to side-force and yawing-moment-due-to- sideslip. Particular attention is paid to the different contributions to the sidewash as experienced by the tail surfaces. Also rudder characteristics are discussed.         POESTELD       E.Obert         DATUM       INTERN AKKOORD         DATUM       INTERN AKKOORD         EXTERN AKKOORD       EXTERN AKKOORD         DATUM       INTERNAL APPROVED         EXTERN AKKOORD       EXTERN AKKOORD         EXTERN AKKOORD       EXTERN AKKOORD         INTERNAL APPROVED       EXTERN AKKOORD         EXTERN AKKOORD       EXTERN AKKOORD         INTERNAL APPROVED       EXTERN AKKOORD         EXTERN AKKOORD       EXTERN AKKOORD         INTERNAL APPROVED       EXTERNAL APPROVED         EXTERNAL APPROVED       EXTERNAL APPROVED         INTERNAL APPROVED       EXTERNAL APPROVED         EXTERNAL APPROVED       EXTERNAL APP	
describes the tail-off characteristics and a part which describes. Particular attention is paid to the side-force and yawing-moment-due-to-sideslip. Particular attention is paid to the different contributions to the sidewash as experienced by the tail surfaces. Also rudder characteristics are discussed.         POESTED       E.Obert         GERANED       E.Obert         INTERNAL APPROVED       EXTERNAL AFPROVED         ENTRAL       INTERNAL APPROVED         EXTERNAL AFPROVED       ECONTROLLED COPY         TERCHING / FOTO NRS.       TER INFORMATIC         FOR INFORMATION       TER INFORMATIC	
tail surfaces to side-force and yawing-incidente due-to scooling reasonance by the tail surfaces.         paid to the different contributions to the sidewash as experienced by the tail surfaces.         Also rudder characteristics are discussed.         POESTELD         REPARED         E.Obert         INTERNAL APPROVED         EXTERNAL AFPROVED         EXTERNAL AFPROVED         EXTERNAL AFPROVED         EXTERNAL AFPROVED         INTERNAL APPROVED         EXTERNAL AFPROVED         EXTERNAL AFPROVED         EXTERNAL AFPROVED         EXTERNAL AFPROVED         EXTERNAL AFPROVED         INTERNAL APPROVED         EXTERNAL AFPROVED	
Also rudder characteristics are discussed.  PCESTELD E.Obert  ITGAVE DATE INTERNAL APPROVED EXTERNAL AFPROVED EXTERNAL A	
PGESTIELD E.Obert  ITGAVE DATE INTERNAL APPROVED EXTERNAL APPROVED	
POESTELD E.Obert CHECKED  INTERN AKKOORD EXTERNAL APPROVED  EXTERNAL A	
PEERTED E.Obert CHECKED	
Intern akkoord     Extern akkoord       SSLE     Date       Date     Internal approved       External approved       Ext	
INTERNAL APPROVED EXTERNAL APPROVED EXTERNAL APPROVED CONTROLLED COPY	
TER INFORMATIE FCR INFORMATION	
TEKENING / FOTO NRS. GRAWING / PHOTO NO'S.   TER INFORMATIE FCR INFORMATION	
TEKENING / FOTO NRS. DRAWING / PHOTO NO'S.	
TEKENING / FOTO NRS. DRAWING / PHOTO NO'S.	
TEKENING / FOTO NRS. GRAWING / PHOTO NO'S.   TER INFORMATIE FCR INFORMATION	
FCR INFORMATION	
FCR INFORMATION	
FCR INFORMATION	-
FCR INFORMATION	
ORDERNS. ORIGINELEN BEWAARD AANTAL BLADEN X Å4 ORDERNO. ORIGINALS FILED NUMBER OF PAGES X Å4	

Form. 3896 12-78 4 EVS/KB (uitv. transparant)

•

:

ţ

# <u>Contents</u>

# Pages

Notation	X - 1 to $X - 7$
Introduction	1
Text	2 to 18
References	19 to 24
Figures referred to in the text	I – 1 to I – 116
Aircraft (Model) geometry and aerodynamic data	II – 1 to II – 68
Determination of $K_{VH}$ , the horizontal tailplane endplate factor	III – 1 to III – 14
Ratio between effective and geometrical vertical tail moment arm	IV-1 to IV- 35
Wind tunnel test data	V-1 to V-35

http://ewade2013.AircraftDesign.org http://dx.doi.org/10.5281/zenodo.21443

# <u>Notation</u>

A	Aspect ratio
$A_{H}$	Horizontal tailplane aspect ratio $b_{H}^{2}/S_{H}$
$A_{V}$	Vertical tailplane aspect ratio $b_V^2 / S_V$
$A_W$	Wing aspect ratio $b_W^2 / S_W$
$b_{FL}, b_{fl}$	Wing flap span
$b_{H}$	Horizontal tailplane span
$b_{\nu}$	Vertical tailplane span ( see page I-19 )
$b_{W}$	Wing span
С	Cross force perpendicular to the X-Z plane, positive to the left.
$C_{C}\left(=-C_{Y}\right)$	Cross force coefficient $C/qS_W$
${\cal C}_H$	Horizontal tailplane chord
$C_{L_{W}}$	Wing ( or tail-off ) lift coefficient $L/qS_{W}$
$C_{L_{T-O}}, (C_L)_{T-O}$	Tail-off lift coefficient
$\mathcal{C}_{l_{lpha}}$	2-dimensional lift gradient due to angle-of-attack
$\mathcal{C}_{l_\delta}$	2-dimensional lift gradient due to control surface deflection
$C_{l_{\rho}}$	Rolling-moment-due-to-sideslip derivative
$\left(C_{I_{\beta}}\right)_{T-O}$	Tail-off rolling-moment-due-to-sideslip derivative
$\left(C_{l_{\rho}}\right)_{\Gamma}$	Contribution to rolling-moment-due-to-sideslip derivative due to wing dihedral
$C_{Llpha}$	Lift-due-to-angle-of-attack gradient (Lift curve slope)
$C_{Llpha_{V}}$	Vertical tailplane lift-due-to-angle-of-attack gradient (Also $\left(C_{Leta} ight)_{\!_V}$ ,)
$C_{L\alpha_{Vest}}$	Estimated isolated vertical tailplane lift-due-to-angle-of-attack gradient

$C_{L\alpha_{V+H}}$ , $C_{L\alpha_{T}}$	Vertical tailplane (including horizontal tailplane endplate effect ) lift-due-to-angle-of-attack gradient. (Also $(C_{L\beta})_{V+H}$ ,) Estimated <u>isolated</u> vertical tailplane (including horizontal tailplane endplate effect ) lift-due-to-angle-of-attack gradient
$C_{L_{\delta_r}}$	Vertical tailplane (including horizontal tailplane endplate effect ) lift-due-to-rudder-deflection gradient
$C_{L_{eta}}$	Rolling moment coefficient due to sideslip
$\left(C_{L_{\beta}}\right)_{V+H}$	See $C_{L\alpha_{V+H}}$
$C_l$	Rolling moment coefficient $\pounds/qS_wb$
$\left(C_{l_{\beta}}\right)_{T-O}$	Tail-off rolling moment coefficient due to sideslip.
$C_n$	Yawing moment coefficient $N/qS_Wb$
<i>C</i> <sub><i>n</i><sub>30</sub></sub>	Yawing moment coefficient with moment reference centre at $x = 0.30\overline{c_w}$ .
$\left(\Delta C_{n_{30}}\right)_{V+H}$	Tail contribution to yawing moment coefficient with moment reference centre at $x = 0.30\overline{c_w}$ .
$C_{n_{\beta}}$	Yawing-moment-due-to-sideslip derivative
$\left(\Delta C_{n_{\beta}}\right)_{FL}$	Contribution to yawing-moment-due-to-sideslip derivative due to flap deflection
$\left(C_{n_{\beta}}\right)_{tail-off}$	Tail-off yawing-moment-due-to-sideslip derivative (Also $(C_{n_{\beta}})_{T-O}$ and $(C_{n_{\beta}})_{WF}$ or $(C_{n_{\beta}})_{WFN}$ .)
$\left(\Delta C_{n_{\beta}}\right)_{T},\left(\Delta C_{n_{\beta}}\right)_{V+H}$	Tail contribution to yawing-moment-due-to-sideslip derivative (Also $\left(C_{n_{\beta}} ight)_{T}$ )
$C_{n_{\delta_r}}$	Yawing-moment-due-to-rudder-deflection derivative
C <sub>r</sub>	Rudder chord
${\cal C}_{R_V}$	Vertical tailplane root chord
$C_{R_{V \exp osed}}$	Exposed vertical tailplane root chord ( see page I-53 )

$C_V$	Vertical tailplane chord
$\overline{c_{\nu}}$	Vertical tailplane mean aerodynamic chord.
$\overline{C_W}$ , $\overline{C_{ref}}$	Wing mean aerodynamic chord.
$C_{\gamma}$	Side force coefficient $Y/qS_W$
$C_{\gamma_{\beta}}$	Side-force-due-to-sideslip derivative
$\left(\Delta C_{y_{\beta}}\right)_{est}$ $\left(C_{y_{\beta}}\right)_{tail-off}$	Estimated tail contribution to side-force-due-to-sideslip derivative ( See pages II-1 to II- 65 ) Tail-off side-force-due-to-sideslip derivative ( Also $(C_{y_{\beta}})_{T-O}$ and $(C_{y_{\beta}})_{WF}$ or $(C_{y_{\beta}})_{WFN}$ ).
$\left(\Delta C_{y_{\beta}}\right)_{FL}$	Contribution to side-force derivative due to flap deflection
$\left(\Delta C_{y_{\beta}}\right)_{nac}$	Contribution to side-force derivative due to engine nacelles
$\left(\Delta C_{y_{\beta}}\right)_{T},\left(\Delta C_{y_{\beta}}\right)_{V+H}$	Tail contribution to side-force-due-to-sideslip derivative (Also $(C_{y_{\beta}})_{T}$ or $(\Delta C_{y_{\beta}})_{VH}$ ).
$\left(\Delta C_{y_{\beta}}\right)_{\Gamma}$	Contribution to side-force-due-to-sideslip derivative due to wing dihedral.
$C_{Y_{\delta_r}}$	Side-force-due-to-rudder-deflection derivative
$\left(C_{y_{\delta_{R}}}\right)_{S_{V}}$	Side-force-due-to-rudder-deflection derivative for a full-vertical-
	tailplane-span rudder derived from side-force data, $Y_{\delta_{ m R}}/q{S_{ m V}\over S_{ m W}}S_{ m W}$
$\left(C_{y_{\mathcal{S}_{R}}}^{*}\right)_{\mathcal{S}_{V}}$	Side-force-due-to-rudder-deflection derivative for a full-vertical- tailplane-span rudder derived from yawing moment data,
	$N_{\delta_{R}} / q \frac{S_{V}}{S_{W}} \frac{l_{VR+(DF)}}{b_{W}} S_{W} b_{w}$
$D_{f_{\max}}$ , $D_{fus}$ , $d$	Maximum fuselage diameter
$d_{\scriptscriptstyle V}$ , $D_{\scriptscriptstyle V}$	Fuselage height as defined on page I-19

$\frac{d\sigma}{d\beta}$	Sidewash-angle-to-sideslip-angle ratio
E	Rudder-chord-to-fin-chord ratio $c_r / c_v$
$h_{\overline{w}}$ , $\ \Delta h_{\overline{w}}$	Wing root height relative to fuselage centre line. Positive when wing is above the fuselage centre line.
i <sub>h</sub>	Horizontal tailplane angle-of-incidence.
i <sub>v</sub>	Vertical tailplane angle-of-incidence
K <sub>i</sub>	Empirical factor defined on page I-15
K <sub>N</sub>	Empirical factor defined on page I-16
K <sub>FV</sub>	Fuselage-vertical-tailplane lift carry-over effect
$K_{VH}$	Horizontal-to-vertical tailplane endplate effect
$K_{V\!H_{est}}$	Estimated horizontal-to-vertical tailplane endplate effect
L	Lift
l <sub>B</sub>	Fuselage length (see page I-16)
$l_{\scriptscriptstyle V}$ , $l_{\scriptscriptstyle V_{ m 30}}$ , $l_{\scriptscriptstyle V}^{\;*}$	Vertical tailplane yawing moment arm measured from $x = 0.30\overline{c_w}$ or $x = 0.25\overline{c_w}$ .
$l_{V+dfn}^{*}$	Effective vertical tailplane yawing moment arm including dorsal fin n. ( n=2,3,4,5 ) For Fokker models measured from $x = 0.30\overline{c_W}$ . (Also $l_{V+DF}$ )
l <sub>Vrsf</sub>	Vertical tailplane moment arm related to reference (=exposed) vertical tailplane area
£	Rolling moment
Ν	Yawing moment
n <sub>nac</sub>	Number of engine nacelles
q	Free-stream dynamic pressure $q = \frac{1}{2}\rho V^2$
$q_{\nu}$	Average dynamic pressure at the vertical tailplane

$R_{TL}$	Tail moment arm ratio ( Tail length ratio) $R_{TL} = \left( \Delta C_{n_{\beta}} \right)_T / - \left( \Delta C_{y_{\beta}} \right)_T * \frac{l_v}{b_w}$
$S_{B_S}$	Body side area (see page I-16)
S <sub>dfn</sub>	Area of dorsal fin n ( n =2,3,4,5 ) (Also $S_{\rm DF}$ )
$S_{\mathit{fus.cross}}$	Maximum fuselage cross section.
$S_H$	Horizontal tailplane are
$S_{\nu}$	Vertical tailplane area ( see page I-19 )
$S_{\nu_r}$	Part of vertical tailplane area affected by the rudder (see page I-19).
$S_{V_{ref}}$	Reference (=exposed) vertical tailplane area
$S_W$ ,	Wing area
$S_{W_{ref}}$	Reference wing area
$S_{W trap}$	Wing area of trapezoidal wing
V	Free stream velocity
$V$ $\overline{V_{\nu_{30}}}$	Free stream velocity Vertical tailplane volume coefficient with moment centre at $x = 0.30 \overline{c_W}$ .
$\overline{V_{\nu_{30}}}$	Vertical tailplane volume coefficient with moment centre at $x = 0.30\overline{c_w}$ . Spanwise position of the centroid of span loading as a fraction of the
$\frac{\overline{V_{\nu_{30}}}}{\overline{y^*}}$	Vertical tailplane volume coefficient with moment centre at $x = 0.30 c_w$ . Spanwise position of the centroid of span loading as a fraction of the semispan.
$\frac{\overline{V_{\nu_{30}}}}{\overline{y^*}}$	Vertical tailplane volume coefficient with moment centre at $x = 0.30c_w$ . Spanwise position of the centroid of span loading as a fraction of the semispan. Distance along fuselage centre line from fuselage nose Distance from fuselage nose of vertical tailplane aerodynamic centre
$\frac{\overline{V_{V_{30}}}}{\overline{y^*}}$ $x$ $x_{acy}$	Vertical tailplane volume coefficient with moment centre at $x = 0.30c_w$ . Spanwise position of the centroid of span loading as a fraction of the semispan. Distance along fuselage centre line from fuselage nose Distance from fuselage nose of vertical tailplane aerodynamic centre including dorsal fin.
$ \frac{\overline{V_{V_{30}}}}{\overline{y^*}} $ $ x $ $ x $ $ x $ $ x $ $ x $ $ x $ $ x $ $ x $ $ x $ $ x $ $ x $ $ x $	Vertical tailplane volume coefficient with moment centre at $x = 0.30c_w$ . Spanwise position of the centroid of span loading as a fraction of the semispan. Distance along fuselage centre line from fuselage nose Distance from fuselage nose of vertical tailplane aerodynamic centre including dorsal fin. Longitudinal position of engine exhausts ( see page I-53 )
$ \frac{\overline{V_{V_{30}}}}{\overline{y^*}} $ $ x $ $ x $ $ x $ $ x $ $ x $ $ x $ $ x $ $ x $ $ x $ $ x $ $ x $ $ x $ $ x $ $ x $ $ x $ $ x $ $ x $	Vertical tailplane volume coefficient with moment centre at $x = 0.30 c_w$ . Spanwise position of the centroid of span loading as a fraction of the semispan. Distance along fuselage centre line from fuselage nose Distance from fuselage nose of vertical tailplane aerodynamic centre including dorsal fin. Longitudinal position of engine exhausts ( see page I-53 ) 0% $x_{R_v}$ = longitudinal position of vertical tailplane root chord

	$z_w  (= -  h_W)$	Wing root height relative to fuselage centre line. Positive when wing is below the fuselage centre line ( see page I-15 ).		
	$lpha$ , $lpha_{_R}$	aircraft angle-of-attack		
	$\alpha_h$	Horizontal tailplane angle-of-attack		
	$\alpha_h^*$	Horizontal tailplane zero-lift angle-of-attack relative to tailplane reference plane		
	$\alpha_{v}$	Effective vertical tailplane angle-of-attack		
	$\frac{\Delta\alpha_{\rm o}}{\Delta\delta}$	2-dimensional control surface effectiveness $\frac{c_{l_{\delta}}}{c_{l_{\alpha_0}}}$ ( see page I-116 )		
	β	Sideslip angle		
	$\Gamma_{W}$	Wing dihedral angle		
	$\delta_{_f}$	Flap angle		
	$\delta_s$	Slat angle		
	$\delta\sigma / \delta\beta$ , $\frac{\delta\sigma}{\delta\beta}$ , $\frac{d\sigma}{d\beta}$	Sidewash-angle-to-sideslip-angle ratio		
	$\left(rac{\delta\sigma}{\deltaeta} ight)_{FV}$	Fuselage-vertical-tailplane interference factor		
	$\left(\Delta \frac{\delta \sigma}{\delta eta} ight)_{h_{W}}$	Effect of relative wing height on the fuselage on the		
	IV IV	sidewash-angle-to-sideslip-angle ratio		
	$\left(\Delta \frac{\delta \sigma}{\delta \beta}\right)_{\Gamma}$	Effect of wing dihedral on the sidewash-angle-to-sideslip-angle ratio		
-	$\left(\Delta \frac{\delta \sigma}{\delta eta}\right)_{\rm FL}$	Effect of wing flap deflection on the sidewash-angle-to-sideslip-angle		
	、 <i>、 、 、 「L</i>	ratio.		
	$\left(\Delta \frac{\delta \sigma}{\delta \beta}\right)_{FL, Ida}$	Effect of wing flap deflection to the landing position on the sidewash-		
	\ FL,ldg			
	( OP ) FL,ldg	angle-to-sideslip-angle ratio.		

(	δσ	
	δβ	) <sub>CIβ</sub>

Effect of rolling moment due to sideslip on the sidewash-angle-to-sideslip-

angle ratio.

the sidewash-angle-to-sideslip-angle ratio

$\left(\Delta \frac{\delta \sigma}{\delta \beta}\right)_{\rm NF}$	Effect of rear-fuselage engine nacelles on the
	sidewash-angleto-sideslip-angle ratio
$\left(\Delta \frac{\delta \sigma}{\delta \beta}\right)_{NW}$	Effect of engine-nacelles-on-the-wing on the
	sidewash-angle-to-sideslip-angle ratio
ε	Downwash angle
λ	Taper ratio
$\lambda_{_H}$	Horizontal tailplane taper ratio
$\lambda_{p}$	Vertical tailplane taper ratio
$\lambda_{w}$	Wing taper ratio
$\Lambda_{\mathcal{H}c_{H}}$	Horizontal tailplane quarter-chord sweep angle
$\Lambda_{\mathcal{H}c_{\mathcal{V}}}$	Vertical tailplane quarter-chord sweep angle
$\Lambda_{\mu c_{\mathrm{IF}}}$	Wing quarter-chord sweep angle
ρ	air density
σ	Sidewash angle

## Model or aircraft components

W,V	wing
F, R	fuselage
N <sub>f</sub> , G	engine nacelles on the rear fuselage
N <sub>w</sub> ,	engine nacelles on the wing
V	vertical tailplane
Н	horizontal tailplane
DR	dorsal fin

All dimensions are measured in m, in, m<sup>2</sup> or in<sup>2</sup>.

Unless otherwise indicated all angles are measured in degrees ( deg ).

### Static Directional Stability and Control of Jet Transport Aircraft

#### Introduction

Static directional stability and control of transport aircraft is primarily determined by the forward fuselage and the vertical tailplane or fin and the rudder with some secondary effects due to the wing and wing-fuselage interference.

For preliminary design purposes the contribution of the forward fuselage can be determined with the standard design manual methods. However, these manuals do not consider the effect of angle-of-attack or high-lift devices on tail-off side force or yawing moment. This effect is addressed in the present report.

Determining the characteristics of the vertical tail surface and rudder is a more complex process. This is due to the vertical tail being positioned in a flow field affected by all other major aircraft components. In a sideslip the fuselage, wing, engine nacelles and even the horizontal tailplane create all different, often non-linear, cross flows, also depending on their relative position. (High - or low - wing, engine nacelles on the wing or on the rear – fuselage, high or low horizontal tailplane.) Furthermore modern transport aircraft have swept wings and highly efficient high-lift systems. This tends to produce large variations in the rolling-moment-due to-sideslip at varying angle-of-attack which in turn produces significant variations in cross flow at the tail.

Standard design manuals such as ESDU Data Sheets and the USAF Datcom and the textbooks derived from these sources consider only fuselage cross flow and the effect of the vertical position of the wing on the fuselage and of the wing dihedral on this cross flow , all at zero angle-of-attack.

In the present analysis the different contributions to the cross-flow or sidewash at the tail mentioned above and not covered by the design manuals are discussed in detail. As the analysis is entirely based on experimental data sometimes large variations in flow characteristics are noted on configurations wit relatively small variations in geometry. Nevertheless an effort is made to present elementary guidelines for the preliminary design of vertical tail surfaces.

The data compilation in this report took place over the years 1978 – 2013. The text was finished in July 2013.

# Some general guidelines for the analysis of directional stability and control of transport aircraft.

With respect to fin and rudder sizing directional stability and control requirements for transport aircraft refer primarily to steady-state conditions. The two main conditions to be considered are:

Crosswind take-offs and landings with maximum crosswind. Maintaining directional control after an engine failure at low airspeeds.

As the information provided in the present report is primarily intended for preliminary design studies, the attention is focused on the low-speed regime.

Tail surfaces perform three functions :

1. They provide static and dynamic STABILITY.

- 2. They enable aircraft CONTROL.
- 3. They provide a STATE OF EQUILIBRIUM in each flight condition.

In general the following DESIGN REQUIREMENTS can be formulated for <u>VERTICAL\_TAIL\_SURFACES</u>:

- 1. They shall provide a sufficiently large contribution to static and dynamic directional STABILITY. This determines primarily their lift SLOPE,  $dC_{L_v}/d\alpha_v x S_V$ .
- 2. They shall provide sufficient CONTROL CAPABILITY  $dC_{L_{v}}/d\delta_{r}xS_{v}$  without flow separation up to high sideslip and rudder deflection angles.
- 3. Control shall be possible with sufficiently LOW CONTROL FORCES either for manual control or to minimize control system weight.

Control Force F =  $C_h x^{1/2} \rho v^2 S_c \overline{c_c}$ .

For a constant rudder area the HINGE MOMENT is MINIMISED when the factor  $S_{o}.\overline{c_{o}} \approx b_{o}.\overline{c_{o}}^{2}$  is minimized.

For all three requirements a MAXIMUM ASPECT RATIO and for HIGH ASPECT RATIOS MINIMUM SWEEP is favourable.

- 4. The vertical tail surface shall be able to cope with HIGH TAILPLANE ANGLES OF ATTACK both with sideslip angle and rudder deflection with equal sign and with opposite sign. In this case a LOW ASPECT RATIO and applying SWEEP is beneficial.
- 5. The tail surface shall be able to provide a MAXIMUM FORCE sufficiently large to BALANCE the total tail-off forces and moments so that STATIC EQUILIBRIUM is achieved in all flight conditions. This leads to specific requirements on TAIL SURFACE AREAS and on the MAXIMUM LIFT COEFFICIENT of the vertical tail with a varying degree of rudder deflection including the effect of ice roughness.

The <u>RUDDER</u> performs three functions :

- 1. It provides a means to achieve a STEADY STATE OF EQUILIBRIUM (TRIM) either at zero or at non-zero control force.
- 2. It allows MANOEUVRING up to maximum yaw rates.

3. It provide a means to COUNTERACT DISTURBANCES, both small and large, such as gusts, which might otherwise cause the aircraft to deviate from its intended flight path (flight path TRACKING).

In order to obtain a MAXIMUM LIFT FORCE due to rudder deflection the use of a deep rudder may be tempting. However, the resulting maximum force and moment increases far from linearly with rudder depth for the larger rudder-to-fin chord ratio's.

Within the normal range of rudder-to-fin chord ratio's (  $c_R/c_V = 0.20$  to 0.35 ) the MAXIMUM SIDE FORCE DUE TO RUDDER DEFLECTION is FAIRLY INDEPENDENT OF FIN SHAPE AND RUDDER DEPTH.

The type of AERODYNAMIC BALANCE on the rudder has a LARGE EFFECT on the DEGREE OF LINEARITY of the variation of the hinge moment due to angle-of-attack and due

to rudder deflection. (  $C_h = C_{H_0} + \frac{\delta C_h}{\delta \alpha_V} \alpha_V + \frac{\delta C_h}{\delta \delta_R} \delta_R$  seldom applies at large angles.)

HORN BALANCES and DORSAL FINS IMPROVE LINEARITY OF HINGE MOMENTS. LONG SPAN OVERHANG BALANCES have an ADVERSE EFFECT on this linearity.

LINEARITY of hinge moments is particularly important for RUDDERS because in sideslips the rudder may be deflected to its maximum angle both to the weather side (during  $V_{MC}$ - tests) and to the lee side (in sideslips and cross-wind take-offs and landings)

#### A special characteristic of vertical tail surfaces

The most stringent design requirement for vertical tail surfaces is the ability to cope with VERY LARGE SIDESLIP ANGLES up to 25 degrees. Therefore vertical tail surfaces have :

- Low aspect ratio's
- Large leading-edge sweep
- sometimes dorsal fins

As shown on page I-21 to I-24 for lifting surfaces with an aspect ratio A  $\leq$  1.5 the lift curve gradient  $C_{L_{\alpha}} = 0.0274$  A. As A = b<sup>2</sup>/S and  $L = C_{L_{\alpha}} \times \alpha \times \frac{1}{2} \rho V^2$  S then

 $L = 0.0274 \,\mathrm{b}^2 \,\mathrm{x}\,\alpha \,\mathrm{x}\,\frac{\gamma_2}{\rho} V^2 \qquad (\,\mathrm{Note}\,\,\alpha = \alpha_\nu = -\beta\,)$ 

Thus: The side force gradient on a fin is to a first order independent of the shape and the fin chord but only of the fin span ( fin height ).

Adding a dorsal fin or applying wing sweep does however often increase the maximum lift and the angle-of-attack for maximum lift and improves the linearity of the aerodynamic characteristics. Therefore a dorsal fin and fin sweep are also beneficial for low-speed aircraft.

#### Tail - off side force and yawing moment

On pages I-1 to I-12 the tail-off side force and yawing moment is presented of a number of aircraft models as obtained from wind tunnel tests. Page I-13 shows for one model, F-29 Model 2-5, the raw data and the sideslip derivatives as given in ref. 59. Ref.59 shows the sideslip derivatives in fig.66b which is reproduced as the lower left figure on page I-13. Reconsidering the slope of the raw data produced slightly different derivatives.( See page I-13 with data from ref.59 figs.34a,b and 35 and the lower left part of page I-12). This illustrates that inaccurate determination of derivatives may lead to confusing conclusions.

The tail-off side force and yawing moment are analyzed in the present report, although in a slightly modified form, according to the method presented in the USAF Datcom and NACA TN D-6946.

In the USAF Datcom the side force is estimated according to the formula :

$$(C_{y_b})_{WFN} = \frac{S_{fus.cross}}{S_W} K_i \frac{2}{57.3} - 0.0001\Gamma - 0.0011 n_{nac}$$

(The latter term is taken from ESDU Data Sheet No. 79006.)

From the data on pages I-8 to I-12 and the lower part of page I-14 it is concluded that flap deflection increases the tail-off side force and decreases the yawing moment and both are slightly affected by angle-of-attack. Although these effects show considerable variations a trend can clearly be observed. Therefore average curves for these changes in tail-off side force and yawing moment due to flap deflection  $(\Delta C_{y_{\beta}})_{FL}$  and  $(\Delta C_{n_{\beta}})_{FL}$  are proposed on the

upper half of page I-14.

For the models in cruise configuration no unambiguous effect of angle-of- attack on side force or yawing moment could be determined.

The test data of Models SKV-LST-3 (page I-11) and SKV-6 (page I-12) with and without engine nacelles on the wing show on average that fitting engine nacelles on the wing produces an increase in side force  $(\Delta C_{y_{\beta}})_{nac}$  =-0.0035 and in yawing moment  $(\Delta C_{n_{\beta}})_{nac}$  = -0.0005 for two engines.

The test data of Models 8/41 (pages I-8, I-9) and SKV-LST-3 (page I-11) with and without engine nacelles on the rear fuselage show on average that two engine nacelles on the rear fuselage produce an increase in side force  $(\Delta C_{y_{\beta}})_{nac}$  =-0.0005 and no effect on yawing

moment( $(\Delta C_{n_{\beta}})_{nac}$ =0) is observed.

C

Based on the analysis of the wind tunnel data as described above the tail-off side force formula is modified to :

$$(C_{y_b})_{WFN} = \frac{S_{fus.cross}}{S_W} K_i \frac{2}{57.3} - 0.0001\Gamma + (\Delta C_{y_p})_{FL} - 0.00175 n_{nac} \text{ (nacelles on wing)}$$
  
- 0.00025 n<sub>nac</sub> (nacelles on fuselage)  
For  $K_i$  see page I-15 For  $(\Delta C_{y_p})_{FL}$  see page I-14 (1)

The tail-off yawing moment in the USAF Datcom is estimated via :

$$(C_{n_{\beta}})_{WFN} = -K_N \frac{S_{B_S}}{S_W} \frac{l_B}{b_W}$$
 with the factor  $K_N$  read off a graph presented on page I-16.

The analysis of the wind tunnel data on pages I-8 to I-14 showed the effect of angle-of- attack and flap angle on the tail-off yawing moment and led to the modified formula:

$$(C_{n_{\beta}})_{WFN} = -K_N \frac{S_{B_S}}{S_W} \frac{l_B}{b_W} + \left( \Delta C_{n_{\beta}} \right)_{FL} \quad \text{with } K_N \text{ taken from page I-16}$$
(2)

On pages I-17 and I-18 a comparison is presented of the tail-off side force and yawing moment for the models in cruise configuration as estimated with the formula given above and data derived from wind tunnel tests.

#### The tail contribution to side force and yawing moment

#### Some definitions

On page I-19 some geometrical definitions concerning the vertical tail surface or fin are presented.

Note that in the definition of area and span (height) the tail surface is assumed to continue inside the fuselage up to the fuselage centre line. This is in accordance with the definition used in most NACA publications and differs from the definition used in the ESDU Data Sheet and used by several aircraft manufacturers.

Page I-20 shows some sketches explaining the flow characteristics in front of the vertical tail affecting the contribution of the tail to side force and yawing moment.

The lift curve slope of isolated lifting surfaces.

On pages I-21 to I-24 lift curve slopes for various lifting surfaces are shown. (3)

These figures clearly show that for low-aspect-ratio surfaces with  $A \le 1.5$  the actual shape (sweep, taper ratio, tip shape) has hardly any effect on the lift curve slope.

# The effect of a dorsal fin on the lift curve slope and the aerodynamic centre of the vertical tailplane.

Pages I-25 to I-38 show the effect of a dorsal fin on the vertical tail characteristics.

Although the main purpose of a dorsal fin is increasing the maximum angle-of-attack of the vertical tailplane before flow separation occurs the tailplane lift gradient is slightly increased and the aerodynamic centre moves forward. These effects can also be seen when leading-edge strakes or leading-edge extensions (LEX) are considered in the wing designs of modern combat aircraft .The data presented are derived from wind tunnel tests performed during the development programmes of both the Fokker F-27 and the F-28.

Page I-35 shows the data derived from the wind tunnel test results of the F-28 Models 8/4 and 8/41.

From the tests on the F-27 tail model only cross force coefficients (= - side force coefficients) were available. (page I-37). The change in lift curve slope due to dorsal fins of different size is indicated in the lower figure on page I-38.

The lower figure on page I-36, taken from test data of a complete F-27 model, shows that for different dorsal fins the yawing moment, at least up to medium yaw angles, is not affected by fin size or shape. This means that the increase in side force due to an increase in fin size is counteracted by a forward movement of the aerodynamic centre. With this in mind this

shift in aerodynamic centre was determined with the data from page I-37. (Upper figure on page I-38)

Note the similarity between the curves for the two data sets on pages I-35 and I-38.

On pages I-25 to I-34 a collection of available raw wind tunnel data and on page I-35 to I-38 a collection of available dorsal fin aerodynamic data is presented.

(4)

#### The endplate effect of the horizontal tailplane on the vertical tailplane lift curve slope.

Wind tunnel test data of the endplate effect of the horizontal tailplane  $K_{\nu H}$  is shown on pages I-39 to I-45.

The lower figure on page I-39 shows a graph of the endplate effect of the horizontal tailplane on the lift curve slope of the vertical tailplane as expressed by a change in effective aspect ratio  $A_{\nu}$  as presented in the USAF Datcom.

Analysis of all available test data, including wind tunnel data on later transport aircraft produced a slightly modified curve (pages I-41 and I-42), in particular for horizontal tailplanes mounted on the fuselage. (page I-45).

The derivation of the individual data points in the figures on pages I-41, I-42 and I-45 can be found in the second part of this report, pages II-1 to II-68. These data are rearranged in a separate chapter on pages III-1 to III-14.

The effect of the tailplane area ratio  $S_H / S_V$  on the endplate effect is shown for a number of configurations on page I-43 together with the average curve given in the USAF DAtcom.

The endplate effect of the horizontal tailplane on the vertical tailplane can be determined with the aid of the graphs presented on page I-39 to I-45.

(5)

The endplate effect of the horizontal tailplane is not only affected by the tailplane relative vertical position and tailplane area ratio but also by the horizontal tailplane effective angle-of-attack or lift coefficient. This is illustrated on page I-44 for a number of model configurations.

It will be clear that a lifting swept horizontal tail surface shows a cross flow above and below the upper and lower surface in a sideslip just as a wing produces a cross-flow and a rollingmoment-due-to-sideslip. It is however not immediately clear what the relation is between the sign of sideslip angle,,tailplane lift coefficient and average cross flow direction at the vertical tailplane.

For the average horizontal tailplane the effect of the tail lift on the endplate effect on the vertical tailplane can be expressed as :  $K_{VH} = (K_{VH})_{\alpha_H=0} \left[ 1 - 0.014 (\alpha_H + \alpha^*) \right]$ 

(6)

Some additional data on the lift curve slope of the vertical tail including the endplate effect of the stabilizer of models SKV-LST-3 and F-29-1-1 are given on pages I-57 and I-58.

#### Sidewash at the vertical tailplane.

#### 1. Sidewash or cross-flow due to the presence of the fuselage.

Sidewash due to the flow around a fuselage in sideslip is illustrated on page I-20.

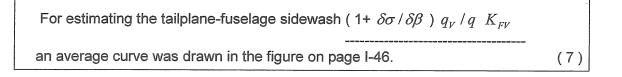
On page I-46 a collection of sidewash data for fuselage-tailplane combinations is shown.

The sidewash parameter is defined as the product of the actual sidewash ratio (1+  $\delta\sigma/\delta\beta$ ), the effective-versus-free-stream dynamic pressure ratio  $q_V/q$  (to take into account the fuselage-boundary-layer effect) and the tailplane-fuselage lift carry-over effect  $K_{FV}$ .

The parameter (1+  $\delta\sigma/\delta\beta$ )  $q_V/q$   $K_{FV}$  is presented as a function of finspan-to-fuselage-diameter ratio  $b_V/d_V$ . (See page I-19 for the definition of  $b_V$  and  $d_V$ )

In the upper figure on page I-39 this fuselage-tailplane interference effect is expressed as a ratio between the nominal and effective vertical tailplane aspect ratio  $(A_{\nu(B)})/(A)_{\nu}$ .

For  $A \le 1.5$  the lift gradient can be written as  $C_{L\alpha} = 0.0274 \ A$  and thus the tailplane aspect ratio given above is equivalent to the fuselage-tailplane interference factor (1+  $\delta\sigma/\delta\beta$ )  $q_V/q$   $K_{FV}$ . Therefore the curves on pages I-39 and I-46 show a high degree of similarity.



#### 2. Sidewash due to wing-fuselage interference. (Rolling moment due to sideslip 1.)

The data on pages I-47 and 48 show the effect of the wing position in height on the fuselage on the sidewash-due-to-sideslip derivative.

$$\left(\Delta \frac{d\sigma}{d\beta}\right)_{h_{W}} \frac{q_{V}}{q} K_{FV} = -0.40 \frac{h_{W}}{D_{f_{\text{max}}}} \quad \text{For definition of } h_{W} \text{ and } D_{f_{\text{max}}} \text{ see page I-19}$$
(8)

#### 3. Sidewash due to wing dihedral and sweep. (Rolling moment due to sideslip II.)

Based on a limited amount of wind tunnel test data (see page I-49) an equation (equation 9) has been found that expresses the relation between sidewash and wing dihedral. Wing dihedral has been substituted by the change in rolling-moment-due-to-sideslip derivative due to wing dihedral  $(\Delta C_{l_{\beta}})_{\Gamma}$  to account for both dihedral an

wing sweep .

$$\left(\Delta \frac{\delta \sigma}{\delta \beta}\right)_{\Gamma} \frac{q_{\nu}}{q} K_{FV} = + \left(110 + 50 \frac{h_{W}}{D_{f_{\text{max}}}}\right) \left(\Delta C_{l_{\beta}}\right)_{\Gamma}$$
(9)

#### 4. Direct sidewash measurements on Model SKV-LST-3.

On model SKV-LST-3 with engine nacelles on the rear fuselage direct sidewash measurements were performed by means of a <u>variable-incidence vertical tailplane</u>. By comparing tail-on and tail-off side-force and yawing moment for different tailplane incidences  $i_{VH}$ , under the assumption that when tail-on and tail-off side-force and yawing moment are equal the load on the tailplane is zero and the average vertical-tailplane

angle-of-attack  $\alpha_{\nu} = 0$ , the average sidewash can be determined via the equation

 $\alpha_{\rm VH}=0=\beta+\sigma+i_{\rm VH} \ \, {\rm or} \ \, \sigma=-\beta-i_{\rm VH}\,. \label{eq:alpha}$ 

Note that to enable variation of the vertical tailplane incidence  $i_{VH}$  a fin root plug was installed (see page II-9b).

Therefore in the analysis two volume coefficients have been used:  $\overline{V} = 0.1443$  for the basic fin including a dorsal fin and  $\overline{V} = 0.1554$  for the fin with rootplug (but without dorsal fin ). The latter configuration was not only used for the tests with variable incidence  $i_{VH}$  but also for tests with varying sideslip angle.

On pages I-57 to I-71 an analysis is presented of the vertical tailplane characteristics as determined according to the method described above On page 57 a detailed analysis is shown for the configuration with engines on the rear-fuselage with flaps and slats retracted at  $\alpha = 0$ .

On the left hand side of page I-57 the vertical tail lift curve slope (including the horizontal

tailplane and dynamic pressure ratio and lift-carry-over effects )  $C_{L_{a_{V+H}}} \frac{q_V}{q} K_{FV}$  is

determined by varying the vertical tailplane incidence  $i_{V+H}$  at sideslip angle  $\beta = 0$ . By

comparing this lift curve slope  $C_{L_{av+H}} \frac{q_V}{q} K_{FV}$  =0.0290 with the theoretical value

 $C_{L_{a_{V+H}}}$  =0.0308 the factor  $\frac{q_{V}}{q}K_{FV}$  =0.942 is obtained.

On the right hand side of page I-57 the sidewash is determined, both from the data on the left side for  $\beta = 0$  (upper right) and by comparing the tail yawing moment contribution  $\frac{dC_{n_{30/H}}}{d\beta} = 0.0048/0.0053$ , as found by varying the sideslip angle  $\beta$  with  $i_{V+H} = 0$ , with the

yawing moment contribution  $\frac{dC_{n_{30/H}}}{di_{V+H}}$  =0.0045 found with  $\beta$  = 0. In both cases  $\frac{\delta\sigma}{\delta\beta}$  = 0.13. Page-58 shows some additional vertical tailplane characteristics.

On the upper half of page I-58 the effect of angle-of-attack and flap deflection on the tail

lift curve slope (including stabilizer)  $C_{L_{a_{V+H}}}$  of model SKV-LST-3 determined at  $\beta = 0$  is presented. This effect is apparently due to variations in local flow direction at the vertical tail resulting in changes in the factor  $\frac{q_V}{q}K_{FV}$ . This is also indicated on page I-71.

The lower half of page I-58 is discussed under the heading. "The effect of engine\_nacelles on the wing on sidewash".

On page I-59 two more examples are shown of the sidewash as determined from tests with different fin incidences on model SKV-LST-3.

Page I-60 shows the overall sidewash results whereas page I-61 shows the change in yawing moment due to fin incidence variation for all model configurations and angles-of-attack investigated .

On pages I-63 / I-64 and I-65 / I-66 the computed sidewash derivative (1+  $\delta\sigma$  /  $\delta\beta$ ) or  $\delta\sigma$  /  $\delta\beta$  and the relative effective dynamic pressure ratio combined with the lift carry-over

factor  $\frac{q_V}{q}K_{FV}$  are presented in tabular form for both the configuration with the fin

including the root plug ( $\overline{V}$  = 0.1554) and with the basic fin ( $\overline{V}$  = 0.1443). On pages I-67, I-69 / I-70 and I-71 this data is presented in graphical form. Page I-68 contains the tail-off rolling-moment-due to-sideslip derivative for the wing-fuselage combination to be used in the analysis of the effect of angle-of-attack and flap deflection on sidewash.

#### 5. Sidewash analysis of other aircraft and windtunnel models.

Besides model SKV-LST-3 a number of wind tunnel models and full-scale aircraft have been analysed according to the method described above :

Fokker 100 Model 15-3 Fokker 100 Model 15-10 Fokker 100 Model 18-5 Fokker 70 Model 15-24 F-29 Model 1-2 F-29 Model 2-5 F-29 Model 5-3 F-29 Model 1-1 F-28 Mk 1000 Model 6-2-3 F-28 Mk 1000 Model 8-3 Airbus A320 Airbus A340 – 300 Douglas DC-9-30 Airbus A300 Boeing 737-100

The results of this analysis are shown on pages I-73 to I-87

6. Sidewash due to rolling-moment-due-to-sideslip

On pages I-69, I-70 and I-73 to I-87 the sidewash term  $\frac{d\sigma}{d\beta}$  as a function of angle-of-

attack  $\alpha_R$ , is presented for all models and aircraft investigated.

The resulting curves show a large variation in shapes, even when for a given aircraft or model the curves derived from side force and yawing moment data are compared. Although some data sets, such as that for Model F-29-1-2 or F-28 Model 8-3, (page I-77 And I-83) show an opposite trend the majority of the curves clearly show a trend where the sidewash diminishes with increasing  $\alpha_R$ . In most cases the curves show a gradual decrease in sidewash, in particular in the normal operating range of  $\alpha_R$ 's. Only at the

highest  $\alpha_R$ 's do the curves drop sharply, presumably due to the beginning of local flow disturbance. No explanation is offered for the smaller downwash at low angles-of-attack in some cases.

Overall however, it is concluded that for preliminary design purposes and lacking other data the decrease in sidewash with increasing angle-of-attack can be expressed with a straight line with a small negative slope.

This effect is attributed to the sidewash resulting from the non-uniform spanwise lift distribution in a sideslip. The upwind wing producing more lift than the downwind wing causes above the wing upper surface a cross flow towards the upward wing decreasing the overall sidewash. This is illustrated on page I-20.

In particular on swept wings the rolling-moment-due-to-sideslip increases with increasing angle-of-attack. (An increasing tendency to roll in an anti-clockwise direction with the wind coming from the right.) This is a linear relation as illustrated in the figures on pages I-89 to I-94.

As for transport aircraft the wing aspect ratio lies usually in the range  $A_{W}$  =7.0 – 12.0 and the wing sweep is mostly  $\Lambda_{W} \leq$  30deg the lift curve slope shows little variation as shown by the table below (complete aircraft).

Aircraft or model	Lift curve gradient	Aircraft or model	Lift curve gradient
Model SKV-LST-3 WF	0.094 / deg	A320	0.093 / deg (AI)
Model SKV-LST-3 WFN <sub>f</sub>	0.095 / deg	A340-300	0.092 / deg (AI)
Model SKV-LST-3 WFNw	0.093 / deg	F-29 model 1-2	0.092 / deg
F-28 model 8-3	0.087 / deg	F-29 model 2-5	0.093 / deg
F-28 model 6-2-3	0.087 / deg	Fo 100 model 15-10	0.090 / deg
		F-27	0.092 / deg

As the lifting –line theory clearly shows the rolling-moment-due-t- sideslip is directly connected to lift and consequently the slope or gradient of the rolling-moment-due-to-sideslip as a function of angle-of-attack will also show little variation with aspect ratio and wing sweep. This is clearly shown in the graphs on pages I-89 to I-94 and the lower figure on page I-108.

On pages I-95 to I-100 the tail-off rolling-moment-due- to-sideslip is presented as a function of the tail-off lift-coefficient. As for the configurations considered the lift curve has a constant gradient with little variation the curves on pages I-95 to I-100 are also straight lines with almost constant gradient.

These gradients  $\left(\frac{C_{l_{\beta}}}{C_{L_{rr}}}\right)$  were computed with equation (12) and compared with the

measured values on page I-111. Note that apart from the data for the A340 calculated and measured data compare reasonably well.

Assuming the relation between the sidewash and the rolling-moment-due-to-sideslip discussed above and the small variation in the rolling-moment-versus- tail-off-lift-coefficient gradient the relation between sidewash and tail-off lift-coefficient is assumed to be linear with a small negative gradient.

In the figures on pages I-102 to I-107 this relation is indicated as a double straight line as an average between the curves derived from side-force and from yawing-moment data. This relation is also described as equation (10).

$$\left(\Delta \frac{\delta \sigma}{\delta \beta}\right)_{Cl\beta} = -0.50 \left[ \left( C_{l_{\beta}} \right)_{T-O} - \left( C_{l_{\beta}} \right)_{T-O,C_{L}=0} \right]$$
(10)

The tail-off rolling-moment-due-to-sideslip is determined with the following equation taken from the USAF Datcom and ref.1 (after some re-writing) :

$$\left(C_{l_{\beta}}\right)_{T-O} = \left(\frac{C_{l_{\beta}}}{C_{LW}}\right) \frac{C_{LW}}{57.3} + \left(\frac{C_{l_{\beta}}}{\Gamma}\right) \Gamma - \left(0.042 \frac{Z_{W}}{D_{fus_{\max}}} + 0.0005 \Gamma\right) \sqrt{A_{w}} \left(\frac{D_{fus_{\max}}}{b_{W}}\right)^{2}$$
(11)

The coefficients which express the effect of wing dihedral and sweep on the rolling-moment-due-to-sideslip  $(C_{I_g} / C_{LW})$  and  $(C_{I_g} / \Gamma)$  are given on pages I-51 and I-52.

The lift-dependent tail-off rolling-moment-due-to-sideslip  $(C_{I_{\beta}} / C_{L_{\pi}})$  may also be determined with the following equation :

$$\left(\frac{C_{I_{\beta}}}{C_{I_{W}}}\right) = -\frac{1}{2} \left[\frac{3}{A_{W}(1+\lambda)} + y^{*} \left(\tan \Lambda_{c/4} - \frac{6}{A_{W}}\frac{1-\lambda}{1+\lambda}\right)\right] + 0.05 \text{ per rad.}$$
(12)

The computed rolling-moment-due-to-sideslip are shown on page I-110.

#### 7. Sidewash due to flap deflection in the landing position

The sidewash due to flap deflection in the landing position is derived from the shift in the figures of the average linearized curves for different flap settings. This shift sometimes showed an increase in sidewash and sometimes a decrease. A similar effect was shown by the rolling-moment-due-to-sideslip. It was therefore concluded that this depended on the relative flap span. This relation is shown in the upper figure on page I-107 and also expressed by equation (13).

For smaller flap angles a sidewash contribution due to flap deflection is assumed to be proportional to the flap angle.

$$\left(\Delta \frac{\delta \sigma}{\delta \beta}\right)_{FL, ldg} = -0.80 \left(\frac{b_{FL}}{b_W} - 0.67\right)$$
(13)

#### 8. The effect of engine nacelles on the wing on sidewash

On the lower half of page I-58 some tailplane data are given for model F-29-1-1. Note that

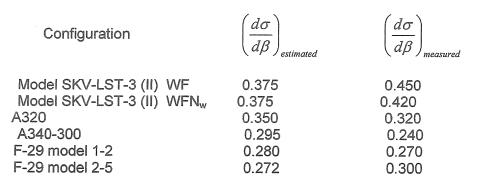
at  $\alpha_R = 0$  fitting the low-set wing  $(h_W / D_{f_{max}} = -0.26$ ,  $\Gamma_W = 7.0 \text{ deg}$ ) and under-wing engine nacelles onto the fuselage-tail combination increases the sidewash by  $\delta\sigma / \delta\beta \approx 0.100$ . Fitting the low-set wing onto the fuselage, together with the wing dihedral

increases the sidewash with  $\Delta \frac{\delta \sigma}{\delta \beta}$  = 0.40x0.26 – (110-50x0.260)x0.00161=

= 0.104 -0.156 = 0.046. See pages I-47, I-49 I-109) and thus on this model fitting two

engine nacelles onto the wings increases the sidewash with  $\left(\Delta \frac{d\sigma}{d\beta}\right)_{NW} \approx 0.145$ 

This seems unlikely given the small increase in sidewash due to the under-wing engine nacelles on model SKV-LST-3 (page I-70) and the small decrease in rolling-moment – due-to-sideslip on models SKV-6 and SKV-6WN (page I-101). Furthermore the sidewash measured on the fuselage +tailplane combination of model1-2 (page II-14b) seems unrealistically low. The available test results on these two fuselage-tail combination are suspect. Also, the estimated sidewash data,computed without any effect of the nacelles (page I-110) and compared with measured sidewash data for the configurations with engine nacelles on the wing show relatively minor differences with either sign (+ or -) as shown in this table :



It is suggested to use the following number as contribution to the sidewash due to under-wing nacelles

$$\left(\Delta \frac{\delta \sigma}{\delta \beta}\right)_{NW} \approx 0$$
-+0.03 (page I-101 and I-103, lower figure) (14)

# 9. <u>The effect of the horizontal and vertical position of rear-fuselage engine nacelles on the sidewash at the vertical tail.</u>

On pages I-53 and I-54 wind tunnel test data are presented of the effect of engine nacelle position on the sidewash-in-sideslip at the vertical tail. The data show for these tests on F-28 Model 8/41 (ref. 22) a considerable effect of relative small variations in nacelle position. If the effect of the dorsal fin on the effective yawing moment arm is incorporated ( $S_{DF}/S_V = 0.071$  and  $l_{V+DF} = l_V 0.95$  see page I-35) the data on side-force and yawing moment compare very well.

Note that the longitudinal position of the nacelles is defined as the distance between the engine exhaust plane and the 0%-point of the fin root chord, positive when the engine exhaust is <u>behind</u> this 0%-point.

The vertical position is defined by the vertical distance between the engine nacelle centre line and the fuselage centre line, positive when the nacelle centre line is above the fuselage centre line.

With the aid of the test data shown on page I-71 the factor  $\frac{q_V}{q}K_{FV}$  was estimated.

By dividing the total sidewash factor (1+  $\frac{\delta\sigma}{\delta\beta}$ )  $\frac{q_v}{q}K_{FV}$  by  $\frac{q_V}{q}K_{FV}$  the true sidewash

factor  $\frac{\delta\sigma}{\delta\beta}$  was found. For the data on pages I-53 and I-54  $\Delta \frac{\delta\sigma}{\delta\beta}$  is given on page I-56.

Generalized curves for estimating the effect of the position of rear-fus	selage
engine nacelles on sidewash-due-to-sideslip at the vertical tailplane $\left(\Delta\right)$	$\Delta \frac{\delta \sigma}{\delta \beta} \bigg _{NF}$ are
given on page 56.	(15)

#### An analysis of the effective tail moment arm.

In the standard approach in analyzing the yawing moment contribution of the vertical tailplane to the aircraft's yawing moment the tailplane side-force is assumed to apply at the 25% m.a.c.-point of the exposed tailplane area. The distance between this point and the moment reference point is considered to be the yawing-moment arm. The analysis of the effect of a dorsal fin on the relation between tailplane side-force and yawing-moment justified an analysis of this relation for tailplanes without dorsal fin as found from wind tunnel tests and in the data bases of some full-scale airplanes.

On pages IV-1 to IV-36 an overview is presented of the ratio

 $R_{TL} = (\Delta C_{n_{\beta}})_{V+H} / (\Delta C_{Y_{\beta}})_{V+H} * \frac{l_{V}}{b}$  in tabular form. On pages I- 112 to I-116 this ratio

is shown in graphical form.

Although a large variation occurs in this parameter it may in general be concluded that the ratio  $R_{\tau t}$  is close to one provided that :

- 1. The data are obtained at a sufficiently high Re-number
- 2. No dorsal fin is fitted
- 3. The rear fuselage is not highly tapered

#### Rudder Characteristics

#### Side- force due to rudder deflection

On pages I-117 to I-120 available data are collected on rudder characteristics of ten aircraft and wind tunnel models. In most cases the side force curves show a linear behavior up to  $\delta_R$ =25 deg. In the normal range of rudder-chord-to-tailplane chord ratio

 $(c_R / c_V = 0.20$ -0.35) the maximum side force is reached at  $\delta_R \approx 35$  deg. The maximum side force loss, relative to the linear  $C_{L_V} - vs. - \delta_R$  relation is then  $\Delta C_{L_V} = 10$  to 15 %. The maximum lift (or side force) is  $C_{L_{V \text{ maxe}}} \approx 0.8$  based on exposed tailplane area or  $C_{L_{V \text{ maxe}}} \approx 0.6$  based on tailplane reference area.

Note that on model SKV-LST-2 a double-hinged rudder was tested. The data on page I-117 refer to the tests with the forward part deflected with the rear part in the neutral position( $c_R/c_V$ =0.311) and with the rear part deflected ( $c_R/c_V$ =0.156).

In order to be able to compare the data of rudders with different relative span the data are normalized to full-span rudders by the ratio  $S_{V_{p}} / S_{V}$  (page I-19).

With the equation given below and the equation for the yawing-moment-due-to-rudderdeflection the ratio  $\frac{(C_{y_{\delta_R}})_{S_V}}{C_{L_{V,V}}}$  (both terms related to the tailplane reference area) were

calculated (page I-121). They are presented in graphical form on page I-122. Note the similarity with the data for two-dimensional flow.

$$(C_{y})_{\delta_{R}} = C_{y_{\delta_{R}}} x \delta_{R} = C_{L\alpha_{V}} x \frac{q_{V}}{q} K_{FV} x K_{VH} x \frac{c_{l\delta}}{c_{l\alpha}} x \frac{S_{V_{R}}}{S_{W}} x \delta_{R}$$
(16)

#### Yawing moment due to rudder deflection

Rudder yawing moment = Rudder side-force x Rudder moment arm. The rudder moment arm is longer than the vertical-tailplane moment arm because the centre-of-pressure of the load due to rudder deflection lies behind the  $0.25\overline{c_v}$  -point.

This difference in distance is  $\Delta l_R \approx 0.30 \, \overline{c_V}$  for the usual range of relative rudder chords. An example is shown on page I-123.

The yawing moment due to rudder deflection can be estimated with equation (17).

$$(C_n)_{\delta_R} = C_{n_{\delta_R}} x \delta_R = C_{L\alpha_V} x \frac{q_V}{q} K_{FV} x K_{VH} x \frac{c_{l\delta}}{c_{l\alpha}} x \frac{S_{V_R}}{S_W} x \frac{l_{V(+DF)} + 0.30\overline{c_V}}{b_V} x \delta_R$$
  
With maximum rudder deflection  $(C_{n_{\max}})_{\delta_R} = 0.90 x C_{n_{\delta_R}} x \delta_{R_{\max}}$  (17)

#### Aircraft (Model) Geometry and Aerodynamic data

On pages II-1a to II-68a detailed geometries are given for all aircraft types and models analyzed in the present report together with the basic available wind tunnel test data As the analysis of the material in this part of the report took place over a long period due to improved insight small differences may be found between some numbers in this part of the report and in the text which was written at a much later date. This refers in particular to some calculations concerning the endplate effect of the horizontal tailplane the conclusions on which were modified in a later stage. These differences have not affected however the overall conclusions.

### **Compilation of Wind Tunnel Test Data**

On pages V-1 to V-35 a compilation is presented of raw wind tunnel test data together with some computed data of all the model tests discussed in this report.

## Some final remarks

1. In the design of transport aircraft the emphasis is on transport capability and thus on performance aerodynamics. In the early phases of the design process the interest is therefore, apart from the fuselage interior arrangement and the loadability, primarily focused on the wing aerodynamics and the airframe-propulsion integration. The interest for the tail surfaces is usually limited to quick estimates of the required volume coefficients for horizontal and vertical tailplanes. This approach may have been adequate when centre-of gravity-ranges were limited and thrust –to-weight ratios were much lower than today but for a modern design with its large c.g.-range, high thrust-to-weight ratio and severe requirements for take-offs and landings with strong cross-winds this approach no longer suffices and a more detailed analysis is required already in an early design stage. The weight but in particular the size of tail surfaces today is such that, in combination with the ever-increasing design range and built-in development potential the role of tailplane sizing in the overall weight and drag prediction is more important than ever.

For horizontal tail surfaces the analysis already goes further than estimating a volume coefficient. With the aid of so-called "scissor plots" the various design requirements for the horizontal tailplane are studied.

The vertical tailplane however, notwithstanding the more complicated flow condition under which the fin has to operate because more airframe components ahead of the fin influence the local flow direction at the fin, has up to now not received the same attention. It is hoped that the present report will help to improve on this unsatisfactory situation.

2. The approach followed in the present report is mainly based on empirical data compilations. As the experience with the USAF Datcom and ESDU data sheets has shown the accuracy of predictions with the information provided in these publications sometimes leaves to be desired.

When no wind tunnel data are available only this empirical approach provides the required sizing information. When wind tunnel data are available on a configuration with a reasonable degree of resemblance more accurate information is obtained when both configurations are analyzed with the data in this report and the difference is added to the data of the older model. Although the actual numbers in the present correlations may not always show the required accuracy the general trends seem reliable.

#### A summary of equations and graphs discussed in this report

Tail-off side force

$$\left(C_{y_{\beta}}\right)_{WFN} = \frac{S_{fus.cross}}{S_{W}} K_{i} \frac{2}{57.3} - 0.0001\Gamma + \left(\Delta C_{y_{\beta}}\right)_{FL} - 0.00175 \,n_{nac} \text{ (nacelles on wing)}$$
  
- 0.00025  $n_{nac} \text{ (nacelles on fuselage )}$   
For  $K_{i}$  see page I-15 For  $\left(\Delta C_{y_{\beta}}\right)_{FL}$  see page I-14 (1)

Tail-off yawing moment

$$(C_{n_{\beta}})_{WFN} = -K_N \frac{S_{B_S}}{S_W} \frac{l_B}{b_W} + \left(\Delta C_{n_{\beta}}\right)_{FL} \quad \text{with } K_N \text{ taken from page I-16}$$
(2)

Lift curve slope of isolated lifting surfaces

On pages I-21 to I-24 lift curve slopes for various lifting surfaces are shown. (3)

#### Dorsal fins

On pages I-25 to I-34 a collection of available raw wind tunnel data and on page I-35 to I-38a collection of available dorsal fin aerodynamic data is presented. (4)

## The endplate effect of the horizontal tailplane on the vertical tailplane

The endplate effect of the horizontal tailplane on the vertical tailplane can be determined with the aid of the graphs presented on page I-39 to I-45.

(5)

For the average horizontal tailplane the effect of the tail lift on the endplate effect on the vertical tailplane can be expressed as :  $K_{VH} = (K_{VH})_{\alpha_{H}=0} \left[ 1 - 0.014 (\alpha_{H} + \alpha^{*}) \right]$ (6)

Vertical - tailplane - fuselage sidewash

For estimating the tailplane-fuselage sidewash ( 1+ $\delta\sigma/\deltaeta$ ) $q_{_V}/q_{_K_{FV}}$		
an average curve was drawn in the figure on page I-46.	(7)	

Sidewash due to wing-fuselage interference

$$\left(\Delta \frac{\delta \sigma}{\delta \beta}\right)_{h_{W}} \frac{q_{V}}{q} K_{FV} = -0.40 \frac{h_{W}}{D_{f_{\text{max}}}} \quad \text{For definition of } h_{W} \text{ and } D_{f_{\text{max}}} \text{ see page I-19. (8)}$$

#### Sidewash due to wing dihedral and wing sweep

$$\left(\Delta \frac{\delta \sigma}{\delta \beta}\right)_{\Gamma} \frac{q_{\nu}}{q} K_{F\nu} = + \left(110 + 50 \frac{h_{W}}{D_{f_{\text{max}}}}\right) \left(\Delta C_{l_{\beta}}\right)_{\Gamma}$$
(9)

Sidewash due to rolling moment due to sideslip

$$\left(\Delta \frac{\delta \sigma}{\delta \beta}\right)_{Cl\beta} = -0.50 \left[ \left( C_{l_{\beta}} \right)_{T-O} - \left( C_{l_{\beta}} \right)_{T-O,C_{L}=0} \right]$$
(10)

Rolling moment due to sideslip

$$\left(C_{l_{\beta}}\right)_{T-O} = \left(\frac{C_{l_{\beta}}}{C_{LW}}\right) \frac{C_{LW}}{57.3} + \left(\frac{C_{l_{\beta}}}{\Gamma}\right) \Gamma - \left(0.042 \frac{Z_{W}}{D_{fus_{\max}}} + 0.0005\Gamma\right) \sqrt{A_{w}} \left(\frac{D_{fus_{\max}}}{b_{W}}\right)^{2}$$
(11)

#### Lift dependent rolling moment due to sideslip

$$\left(\frac{C_{l_{\beta}}}{C_{L_{W}}}\right) = -\frac{1}{2} \left[\frac{3}{A_{W}\left(1+\lambda\right)} + y^{*} \left(\tan\Lambda_{c/4} - \frac{6}{A_{W}}\frac{1-\lambda}{1+\lambda}\right)\right] + 0.05$$
 per rad (12)

#### Sidewash due to flap deflection to the landing position

$$\left(\Delta \frac{\delta \sigma}{\delta \beta}\right)_{FL,ldg} = -0.80 \left(\frac{b_{FL}}{b_W} - 0.67\right)$$
(13)

The effect of engine nacelles on the wing on sidewash

$$\left(\Delta \frac{\delta \sigma}{\delta \beta}\right)_{NW} \approx 0 - 0.04 \quad \text{(page I-100 and I-101)} \tag{14}$$

# The effect of rear-fuselage engine position on sidewash

Generalized curves for estimating the effect of the position of rear-fuselage engine nacelles on sidewash-due-to-sideslip at the vertical tailplane  $\left(\Delta \frac{\delta \sigma}{\delta \beta}\right)_{NF}$  are given on page 56. (15)

Side force due to rudder deflection

$$(C_{y})_{\delta_{R}} = C_{Y_{\delta_{R}}} x \delta_{R} = C_{L\alpha_{V}} x K_{FV} \frac{q_{V}}{q} x K_{VH} x \frac{c_{l\delta}}{c_{l\alpha}} x \frac{S_{V_{R}}}{S_{W}} x \delta_{R}$$

$$With maximum rudder deflection (C_{Y_{max}})_{\delta_{R}} = 0.90 x C_{Y_{\delta_{R}}} x \delta_{R_{max}}$$
(16)

Yawing moment due to rudder deflection

$$(C_n)_{\delta_R} = C_{n_{\delta_R}} x \delta_R = C_{L\alpha_V} x K_{FV} \frac{q_V}{q} x K_{VH} x \frac{c_{l\delta}}{c_{l\alpha}} x \frac{S_{V_R}}{S_W} x \frac{l_{V(+DF)} + 0.30\overline{c_V}}{b_V} x \delta_R$$

$$\text{With maximum rudder deflection} \quad (C_{n_{\max}})_{\delta_R} = 0.90 x C_{n_{\delta_R}} x \delta_{R_{\max}}$$

$$(17)$$

**REFERENCES** 

1. NASA TN D-6946	Lateral-directional aerodynamic characteristics of light, twin-engine, propeller-driven airplanes.
2. NACA Report 1098	Methods for calculating lateral stability and estimating stability derivatives.
3. NASA TN D-8512	Theoretical and experimental analysis of longitudinal and lateral aerodynamic characteristics of skewed wings at subsonic speeds to high angles of attack.
4. NACA TN 1050	Wind-tunnel investigation of endplate effects of horizontal tails on a vertical tail compared with available theory.
5. NACA Report 1171	Effect of horizontal-tail span and vertical location on the characteristics of an unswept tail assembly in sideslip.
6. NACA TN 2010	Effect of horizontal tail on low-speed static lateral stability characteristics of a model having 45° sweptback wing and tail surfaces.
7. Fokker Report no. L-307-59	Aerodynamic characteristics of low-speed windtunnel model SKV-LST - 3 September 1979.
8	Windtunnel test data of the VFW-Fokker 614.
9. NACA RM L57B19	An analysis of vertical tail loads measured in flight on a swept-wing bomber airplane.
10. NASA TM X-74011	Wind-tunnel results of the aerodynamic characteristics of a 1/8 –scale model of a twin-engine short haul transport. (Boeing 737-100) April 1977.
11	Aerodynamic data of the Douglas DC-9-30.
12	Airbus A-300 B-2 Données Aerodynamiques.
13	Airbus A320 Données Aerodynamiques.
14	Airbus A340 – 300 Données Aerodynamiques
15. NACA RM A56I04	The static and dynamic-rotary stability derivatives at subsonic speeds of an airplane model with an unswept wing and a high horizontal tail. (Lockheed F-104 A) September 1956.
16. NACA TN 2488	Wind-tunnel investigation of the contribution of a vertical tail to the directional stability of a fighter-type airplane. (Grumman F6F Hellcat)

17. NLR Report A-1636	Low-speed wind tunnel tests (without and with ground ground plate) on an all-metal model of the F-28 (model 8-3) mainly concerning the flap configurations, the ailerons and spoiler-ailerons, the liftdumpers, the airbrakes and the rudder. (Fokker F-28 Mk 1000)
18. NLR Report T-111	Windtunnel tests, carried out in the HST on the 1 : 20 scale model 6-2-3 of the Fokker F-28. (Fokker F-28 Mk 1000)
19. NLR Report A-1568	Low-speed windtunnel investigation of a model of the F-28 fuselage (model 4, scale 1:10 and 1 : 11.58) With nacelles and airbrakes.
20. NLR Report A-1571	Low-speed wind tunnel investigation on a model of the F-28 fuselage (scale 1: 11.58) with airbrakes and provisional tail surfaces.
21. NLR Report A-1582	Low-speed windtunnel investigation on a model of the F-28 on a scale 1 : 11.58. (model 8/4) June 1966.
22. NLR Report A-1587	Low-speed windtunnel investigation on a complete model of the F-28 on a scale 1 : 12. (model 8/41)June 1966.
23. NLL Report A – 1403	Onderzoek aan het $F - 27 : 6$ - componenten model (1:15) met verlengde romp juli 1955.
24. NLL Report A – 1415	Onderzoek aan het $F - 27 : 6 - componenten model$ (1:15) met een rompverlenging vóór de vleugel.
25. Fokker Report L-27-82C	Aerodynamic characteristics of the $F - 27$ , derived from the "DNW power - off" test. Volume C : Lateral – directional stability and directional control characteristics of the $F - 27$ RE with Mk 200 fuselage length.
26. NLL Report A – 1394	F – 27 Staartvlakkenmodel (1:9) II. Eigenschappen van het verticale staartvlak.
27. NLR Report T-94	Wind tunnel tests carried out in the HST on the 1 :10 scale model 9-1 ( T-tail configuration ) of the Fokker F-28
28. NLR Report T-117	Wind tunnel tests, conducted in the HST, on the 1:10 scale «tail-surface» model (model 9-2) of the Fokker F-28.
29. NACA RM No. A7H12	Force tests of the Boeing $XB - 47$ full – scale empennage in the Ames 40 - by $80 - foot$ wind tunnel August 1947.

30. NACA WR L-12 (NACA ARR L4E25)	<ul> <li>Investigation of effect of sideslip on lateral stability characteristics.</li> <li>I - Circular fuselage with variations in vertical – tail area and tail length with and without horizontal tail surface May 1944.</li> </ul>
31. NACA WR L – 8 (NACA ARR L5C13)	<ul> <li>Investigation of effect of sideslip on lateral stability characteristics.</li> <li>II - Rectangular midwing on circular fuselage with variations in vertical tail area and fuselage length with and without horizontal tail surface.</li> <li>April 1945.</li> </ul>
32. NACA WR L-520	<ul> <li>Wind – tunnel investigation of effect of yaw on lateral – stability characteristics.</li> <li>IV - Symmetrically tapered wing with a circular fuselage having a wedge – shaped rear and a vertical tail.</li> </ul>
33. NACA TN 730	<ul> <li>Wind – tunnel investigation of effect of yaw on lateral – stability characteristics.</li> <li>II - Rectangular N.A.C.A. 23012 wing with a circular fuselage and a fin.</li> </ul>
34. NACA Report No. 705	Wind – tunnel investigation of effect of interference on lateral – stability characteristics of four NACA 23012 wings, an elliptical and a circular fuselage and vertical fins.
35. NACA TN 804	Wind – tunnel investigation of the effect of vertical position of the wing on the side flow in the region of the vertical tail.
36. NACA Report 1049	Experimental investigation of the effect of vertical – tail size and length and of fuselage shape and length on the static lateral stability characteristics of a model with 45° sweptback wing and tail surfaces.
37. NACA TN 3135	Investigation of mutual interference effects of several vertical – tail – fuselage configurations in sideslip.
38. NACA TN 3649	Static longitudinal and lateral stability characteristics at low speed of unswept – midwing models having wings with an aspect ratio of 2, 4, or 6.

39. NACA TN 3857	Experimental investigation at low speed of the effects of wing position on the static stability of models having fuselages of various cross sections and unswept and 45° sweptback surfaces.
40. NACA TN 2504	Effects of wing position and horizontal tail position on the static stability characteristics of models with unswept and 45° sweptback surfaces with some reference to mutual interference.
41. NACA TN 3961	Effects of fuselage nose length and a canopy on the static longitudinal and lateral stability characteristics of 45° sweptback airplane models having fuselages with square sections.
42. NACA TN 3551	Experimental investigation at low speed of effects of fuselage cross section on static longitudinal and lateral stability characteristics of models having $0^{\circ}$ and $45^{\circ}$ sweptback surfaces.
43. NACA RM L56E29	Investigation at high subsonic speeds of the static lateral and directional stability and tail – loads characteristics of a model having a highly tapered swept wing of aspect ratio 3 and two horizontal – tail positions.
44. NACA RM L55J25	Wind – tunnel investigation at high subsonic speeds of some effects of fuselage cross – section shape and wing height on the static longitudinal and lateral stability characteristics of a model having a 45° swept wing
45. NACA RM L56B10	Investigation at high subsonic speeds of the effect of horizontal – tail location on longitudinal and lateral stability characteristics of a complete model having a sweptback wing in a high location.
46. NACA RM L57I13	Static lateral characteristics at high subsonic speeds of a complete airplane model with a highly tapered wing having the 0.80 chord line unswept and with several tail configurations.
47. NACA Report TR 1171	Aerodynamic characteristics of an unswept tail assembly in sideslip.
48. NACA TN 3818	Windtunnel investigation to determine the horizontal- and vertical –tail contribution to the static lateral stability characteristics of a complete-model swept-wing configurationat high subsonic speeds.

49.	NACA	TN 4077	Static longitudinal and lateral stability characteristics at low speed of 45° sweptback-midwing models having wings with an aspect ratio of 2, 4, and 6.
50.	NACA	TN 4397	Static longitudinal and lateral stability characteristics at low speed of 60° sweptback-midwing models having wings with an aspect ratio of 2, 4, and 6.
51.	NACA	RM L 53J19	An experimental and theoretical investigation at high subsonic speeds of the effects of horizontal tail height on the aerodynamic characteristics in sideslip of an unswept. untapered tail assembly.
52.	Fokker	Report L-307-24	Test results of the low-speed windtunnel model $SKV - LST - 1$ .
53.	Fokker	Report L-307-46	Aerodynamic characteristics of the low-speed windtunnel model $SKV - LST - 2$ .
55.	Fokker	Report L-29-118	Aerodynamic characteristics of a high-speed F-29 windtunnel model - Model $1-1$ .
56.	Fokker	Report L-29-135	Aerodynamic characteristics of an H.S.T. model $-$ Model $1-2$ .
57.	Fokker	Report L-29-128	Aerodynamic characteristics of a high-speed F29 windtunnel model - Model 2-1
58.	Fokker	Report L-29-137	Aerodynamic characteristics of an HST model - Model 2-2
59.	Fokker	Report L-29-150	Aerodynamic characteristics of a high-speed $F - 29$ windtunnel model - Model $2 - 5$ .
60.	Fokker	Report L-29-181	Aerodynamic characteristics of a high-speed $F - 29 / MDF - 100$ windtunnel model - Model $5 - 3$ .
61.	NACA	RM L53J19	An experimental and theoretical investigation at high subsonic speeds of the effects of horizontal-tail height on the aerodynamic characteristics in sideslip of an unswept, tapered tail assembly.
62.	NACA	TN 3818	Wind-tunnel investigation to determine the horizontal- and vertical-tail contributions to the static lateral stability characteristics of a complete-model swept-wing configuration at high subsonic speeds.
63.	NACA	TN 4397	Static longitudinal and lateral stability characteristics at low speed of 60° sweptback-midwing models having wings with an aspect ratio of 2, 4, or 6.

64. Fokker Report L-307-56	Aerodynamic characteristics of high-speed wind-tunnel model SKV - 6
65. Fokker Report L-307-70	Aerodynamic characteristics of high-speed wind-tunnel model SKV – 6 – WN 1
66. NLR TR 68095 C	Low-speed wind tunnel tests on stretched version models of Fokker F-28 aircraft (model 8-4 and other), including a so- called "deep stall' investigation.
67. NLR Report T.62	Wind tunnel tests, carried out in the HST on the 1:20 scale models 1 and 2 of the Fokker F-28. Dec.1961 – May 1962
68. Fokker Report L-290-6	Description of the wind tunnel models 1 and 2 for Fokker project 290.
69. Fokker Report L-28-322	Aerodynamic characteristics of the P-332 related F-28 model, Model 15-3.
70. Fokker Report L-28-350	Aerodynamic characteristics of the F-28 Mk 100 model, Model 15-10.
71. Fokker Report L-28-350	Aerodynamic characteristics of, Model 18-5.
72. Fokker Report L-28-522	Windtunnel test results of a F-28 Mk0070 configuration model, Model 15-24.
73. NLL Rapport A-1374	F 27: Onderzoek van een vliegtuigmodel, schaal 1 : 15. IV. Rompweerstand; eigenschappen van verschillende horizontale en verticale staartvlakken, vliegeigenchappen in start, landing en kruisvlucht.
74. Fokker Report L-307-56	Aerodynamic characteristics of high-speed wind-tunnel model SKV- 6.
75. Fokker Report L-307-70	Aerodynamic characteristics of high-speed wind-tunnel model SKV- 6-WN 1.
76. Fokker Report L-28-153	Loads on F-28 empennage as derived from pressure distribution measurements on model 6/2-1, 1965.

